The Canadian Society for Bioengineering
The Canadian society for engineering in agricultural, food, environmental, and biological systems.

CSBE | SCGAB

La Société Canadienne de Génie Agroalimentaire et de Bioingénierie
La société canadienne de génie agroalimentaire, de la bioingénierie et de l'environnement

Paper No. : CSBE08170

MODELING SOIL BEHAVIOUR DURING SUBSOILING

Fangliang Chen
Ying Chen*

*Department of Biosystems Engineering, University of Manitoba, Winnipeg, MB, Canada R3T 5V6; *phone: 204-474-6292; fax: 204-474-7512; e-mail: ying_chen@UManitoba.ca*

ABSTRACT

Information on soil dynamic behaviour of a tillage tool is very important to the evaluation of the performance of the tool and to the design and selection of the tool. A discrete element model was developed to simulate the subsoiling process of a ripper. The model had a field scale and was computed using the commercial code, PFC^{3D}. This PFC^{3D} model predicts the soil cutting forces and soil loosening of the ripper (a single tool) in a clay soil at different travel speeds and tillage depths. The model parameters included soil physical properties (such as initial soil bulk density and the range of soil aggregate sizes) and soil mechanical properties (such as the bond between soil aggregates and friction coefficient of soil-tool). To calibrate and validate the PFC^{3D} model, field tests of a ripper implement were performed in a clay soil condition. The ripper was operated at a tillage depth of 300 mm and travel speeds of 3 km/h. Field measurements included soil physical properties, soil cutting pressures, and soil loosening.

The particle bonding properties were calibrated using an inverse approach by matching the model outputs with the field measurements in soil cutting pressures. The preliminary results showed that the young's modulus of the bond should be between 10^5 and 10^6 Pa, which resulted in the best match between the measured soil cutting pressures and predicted pressures. The model predictions in soil cutting forces will be validated against the existing soil cutting theories, the universal earthmoving equation. The model predictions in soil loosening are to be validated against the field measurements. The model results and the validations will be reported in the future papers.

Keywords: Discrete element, PFC, modeling, ripper, subsoiling, draft, soil, porosity.

INTRODUCTION

Understanding soil-tool interactions has been recognised as the prerequisite for the improvement of exiting tillage tools and for the development of new high-performance tillage tools. Many theoretical methods have been developed for modeling soil-tool interactions occurring in tillage processes. These methods can be divided into two categories: analytical and numerical methods. The analytical methods are simpler and fairly accurate. The passive earth pressure theory was commonly used in analytical methods (Hettiaratchi and Reece 1967; Godwin and Spoor 1977; McKyes and Ali 1977; Perumpral et al. 1983). Majorities of numerical models used finite element methods (Shen and Kushwaha 1998; Chi and Kushwaha 1989). Because tilling soil involves a flow of soil particles around the tillage tool, the discrete element method (DEM) is a promising method for the simulation of soil-tool interactions in soil cutting and tillage, such as subsoiling.

The DEM has been used to simulate the flow of other biological products with the objective of improving the design and performance of material handling and processing machines (Tijskens et al. 2003), since the DEM was first introduced by Cundall and Strack (1979) in the field of rock mechanics. Examples include using the DEM to model the flows of grain in a silo (Lu et al. 1997), solid manure in a spreader (Landry et al. 2006), and rice on a shaking separation plate (Sakaguchi et al. 2001). The DEM has been also used to simulate soil behaviours and soil-machine interactions (Anandarajah 1994; McDowell and Harireche 2002). In the DEM, the physical media of interest (e.g., soil particles) are modeled as collections of particles with each interacting with its neighbouring particles as well as with the physical boundaries of the modelled environment, such as a machine.

The advantages of using the DEM include the availability of computing power and commercial discrete element code, such as the software package: Particle Flow Code in three Dimensions (PFC^{3D}) (Itasca Consulting Group Inc., Minneapolis, USA). A basic PFC^{3D} model is constructed of spherical *balls* which simulate the particles of the material to be modeled. The PFC^{3D} model is capable of dealing with hundreds or thousands of balls, depending on the application. Assembly of balls is placed into *walls* which simulate the physical boundaries of the modeled environment. The walls confine the balls, so that different numbers of balls can be placed into the boundary to achieve the desired porosity of the material to be simulated. Within the model boundary, each ball can contact with several other balls. As the individual balls move, the dynamics of the assembly changes as well. PFC^{3D} has been used as the discrete element code to model solid manure handling and application equipment (Landry et al. 2006), screw conveyors (Shimizu and Cundall 2001), and densification of corn stover grinds (Mani et al. 2006). Lately, van der Linde (2007) used PFC^{3D} to model soil behaviours resulting from a vibratory subsoiler.

This study aimed to simulate soil cutting forces, soil loosening of a subsoiling tool using PFC^{3D}. Subsoiling has been recognized as an effective practice to loosen compacted soil (Busscher et al. 2006) and increase the crop yield (Botta et al. 2006). However, subsoilers require high tractor power (Karlen et al. 1991; Chen et al. 2005), which has slowed the adoption of this tillage practice.

PFC^{3D} simulations will provide important insight into the dynamic and mechanic behaviour of soil-tool interaction in subsoiling processes. This will enhance the understanding of the working parameters in relation to the soil cutting forces and soil loosening, which are important to minimize power requirement of tools and to maximise the soil loosening benefits to plant root development and water infiltration in clay soil conditions. This will ultimately lead to the design of improved subsoiling tools.

The only PFC^{3D} model for tillage tool-soil interaction was developed by van der Linde (2007) who investigated the draft force of a vibratory subsoiling tool and the kinetic energy of soil particle during the vibrating of the tool. The limitations of that study included the tool being powered (not common in North America), dry sandy loam soil condition, simplified version of a real subsoiling tool, focusing on effects of soil properties only. The objectives of this study were (1) to develop a PFC^{3D} model to predict the soil cutting force and soil loosening of a field-scale subsoiling tool (ripper) working in a clay soil condition, as affected by tillage depth and tillage speed, (2) to calibrate some model parameters (e.g. properties of bond between soil particles), and, (3) to validate the model with field measurements, and also with results from the universal earthmoving equation of soil cutting tools.

MODEL DEVELOPMENT

The PFC^{3D} model development included defining the following components and parameters: an assembly of soil particles, contact behaviour, a field-scale virtual tool, a physical region, soil properties, boundary and initial conditions, and outputs.

Soil particles

In soil-tool interaction studies in agriculture, it is more logical to deal with soil aggregates than individual soil particles. Thus, in the PFC^{3D} model, the soil "particles" are referred to as soil aggregates, although the genetic term, particle is being used in the paper. The equivalent term of particles are "balls" in PFC^{3D}. Spherical balls, the fundamental geometry for the discrete-element calculations in PFC^{3D}, were assumed to represent for soil particles, although soil particles are not necessary spherical. Clumps or clusters can be formed in PFC^{3D} to simulate the shape of soil particles. However, there were no needs to use clumps or clusters, because one used the parallel bond model in which all particles are bonded together. The parallel bond model is explained in the following section. In the PFC^{3D} model, the particle sizes varied within a range from R_1 to R_2.

Contact force between particles

Clay is cohesive and certain strength exists between particles, which may resist forces and moments. Thus, particles may be bonded together at the contact. In such a case, a bonding model should be used for clay. PFC^{3D} has two built-in bonding models: contact-bond and parallel-bond. The contact-bond reproduces the effect of adhesion acting over the contact area. When the tensile normal or shear contact force exceeds the respective strength, the bond breaks and the contact forces become zero. The parallel bond provides a connection between two particles that resists both forces and moments applied to the particles. When the respective strengths at the contact area are exceeded, bonds break and the contact forces and moments become zero. For details, readers are referred to Itasca (2005a,b). The parallel bond model was chosen in this

study, because simulation of a subsoiler in a clay soil may need to consider both forces and moments between particles. van der Linde (2007) compared both bonding models and concluded that the parallel bond model was more suitable for simulating soil brittle behaviour observed in the experiment of subsoiling.

Virtual tool

The ripper (Fig. 1a) modeled featured a vertical shank and narrow foot. The shank was edge-on type and the cross-section was 30 x 150 mm. The shank had a '>' shape cutting edge for the purpose of reducing draft. The foot was a narrow point type with a tip. Thus, the ripper had three surfaces which directly cut soil. Those cutting surface were the '>" shape edge and top surfaces of the foot and the tip. In the PFC^{3D} model, 13 "walls" were used to build the virtual ripper (Figs. 1b and 1c) in the field scale. The components of the real ripper and virtual ripper model and their corresponding dimensions are listed in table 1. Every component of the virtual ripper was symmetrical along the X-axis in the coordinate system.

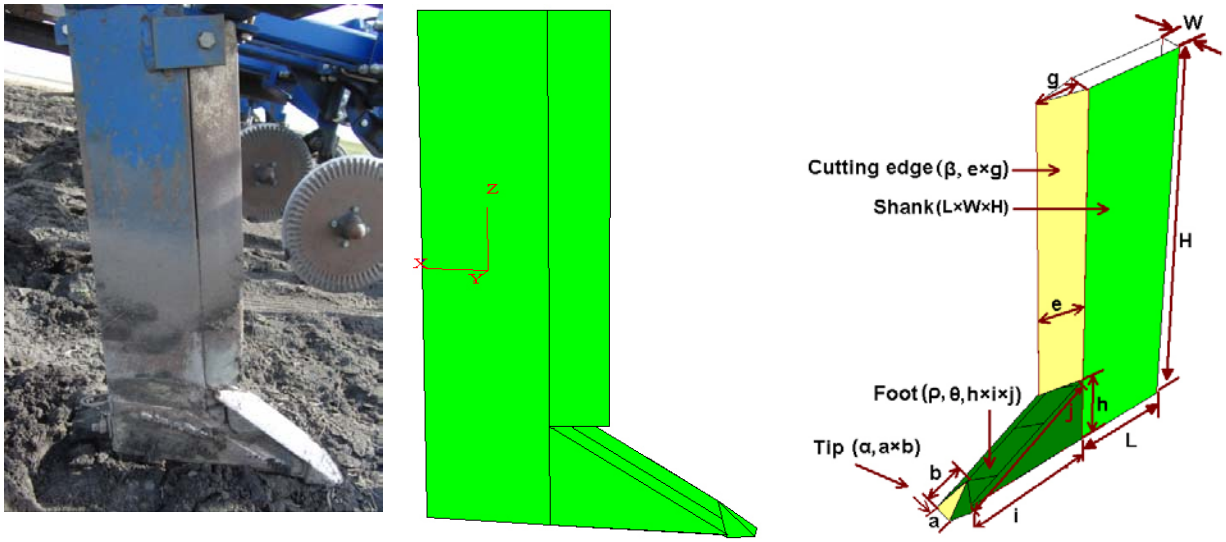

(a) (b) (c)

Fig. 1. Tool geometry of the ripper; (a) photo of the ripper tool (side view); (b) side view of the virtual tool and coordinate; (c) 3D-front-top-view of the virtual tool with dimension symbols.

Table 1. Components of the ripper and virtual ripper and their corresponding dimensions

Parameter and symbol	Description and unit	Value
Shank dimension		
L	Length (mm)	150
W	Width (mm)	30
H	Height (mm)	680
Cutting edge		
β	Angle between two edges (º)	25
e	Length of bevel edge (mm)	70
g	Vertical line of cutting edge (mm)	68
Foot		
θ	Angle relative to ground surface (º)	30
ρ	Angle of foot wing relative to XZ plane (º)	27
h	Foot height (mm)	120
i	Foot length (mm)	210
j	Length of foot bevel edge (mm)	242
Tip		
α	Angle relative to ground surface (º)	57
a	Bottom line of the tip triangle (mm)	30
b	Height of the tip triangle (mm)	57

Physical region of the PFC^{3D} model

In a field implement, rippers are spaced equally on the toolbar as shown in Fig. 2a. The dimension of the tool spacing of subsoiling equipment is usually large, ranging from 0.75 to 0.9 m. The large tool spacing is for reducing the power required by the subsoiling. The tool spacing is large enough, so that there are no interactions between tools, in terms of soil disturbance. It is logical to define the lateral dimensions of the physical region as the midlines (hypothetical lines) between two consecutive rippers in the lateral direction (Fig. 2b). The vertical dimension of the physical region should be greater than the tillage depth, ranging from 0.3 to 0.4 m for typical subsoiling operations. The longitudinal dimension is arbitrary, depending on the computer power, but it should allow for the ripper to reach its stable conditions in terms of forces and soil disturbance.

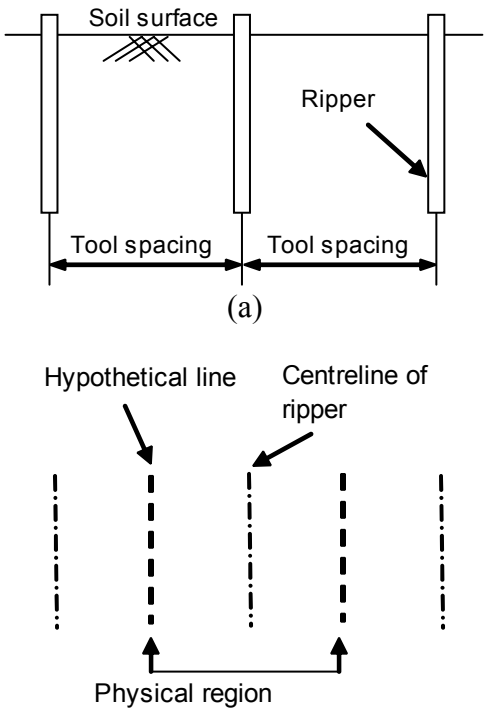

Fig. 2. Diagram showing (a) soil cross-section; (b) Physical region of the PFC^{3D} model.

The physical region in the PFC^{3D} model was selected as 0.9x0.6x0.7 m (width x depth x length) which was large enough to avoid the edge effect on the particle flow. The physical region was represented by a soil box built using six "walls" (Fig. 3). The soil particles ("balls") are placed in the box as described below.

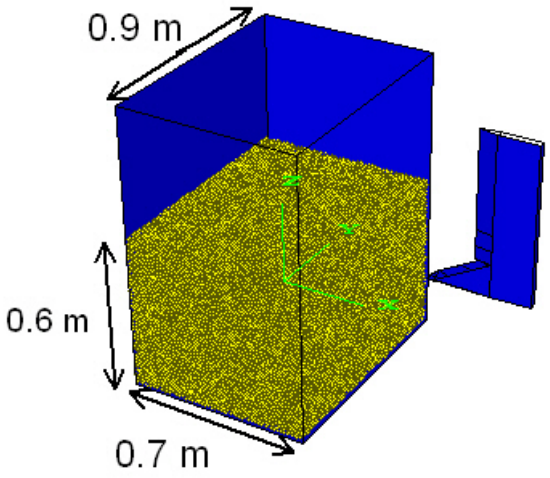

Fig. 3. Particles generated within a soil box.

An initial range of particle radii and initial particle porosity need to be selected. If pore spaces between the soil aggregates are considered as macropores and those between the individual particles within an aggregate are considered to be micropores, the term, porosity, in PFC^{3D} should be equivalent to the term of macroporosity. This is because the porosity in PFC^{3D} is defined as the ratio of the volume of void between balls in a region to the total volume of that region. Thus, the model input for initial porosity should be the soil initial macroporosity, rather than total porosity.

FIELD MEASUREMENTS

Field test of the ripper

To calibrate and validate the PFC^{3D} model, field tests of the ripper (Fig. 1a) were conducted in a clay soil. The field was located at a farm in Oakville, Manitoba, Canada. The soil texture was: 61.7% clay, 35.9% silt, and 2.4% sand by mass. The previous crop was edible bean and the surface soil condition before is shown in Fig. 4a. Seven shanks were mounted on a 6.3-m toolbar (Fig. 4b) at a tool spacing of 0.9 m. In the front of each shank, there was a coulter for cutting crop residue. Effects of the coulter on soil disturbance were considered negligible. The soil surface condition after subsoiling is shown in Fig. 4c.

(a) (b) (c)

Fig. 4. Field condition and field equipment; (a) soil surface condition before subsoiling; (b) ripper subsoiler with seven shanks; (c) soil surface condition after subsoiling.

Field measurements

Initial soil condition Before subsoiling, soil cores (50 mm diameters) were taken at six locations to a depth of 0.4 m at 0.05 m depth intervals. Soil cores were weighed, oven dried at 105 °C for 24 hours, and weighed again to determine initial soil porosity (ASABE 2007) and other soil background information, including soil moisture content.

Soil cutting pressure Soil cutting pressures of the ripper were measured using FlexiForce film pressure sensors (Fig. 5a) (Tekscan Inc., South Boston, MA, USA). The sensor had a sensing circle of 4.76 mm radius, giving a sensing area of 71.26 mm^2 and was able to measure force up to 4533 N. It only measured the soil resistant forces in the normal direction that were perpendicular to the sensing circle plane. The measurement result was recorded as force. It was then converted to pressure for the calibrations and comparisons with the PFC^{3D} model results.

The sensors were installed at three different cutting surfaces on the ripper, with Sensor #1 being on the tip, Sensor #2 on the foot, and Sensor #3 on the shank (Fig. 5b). Sensors were fixed and protected by tapes. The signals of those three sensors were recorded by the Wireless ELF Force Measurement System, including windows-compatible software, a USB-powered Hub, and a battery-operated Transmitter. A laptop computer was used to record the signals. Measurements were performed during two passages of the ripper at a travel speed of 3 km/h. When the ripper travelled with an uniform subsoiling speed of 3 km/h, force data were started to collect from each sensor simultaneously and lasted for about 60 seconds. This gave a travel distance of about 50 m. Higher speed could not be achieved due to the limited horsepower of the tractor.

(a)

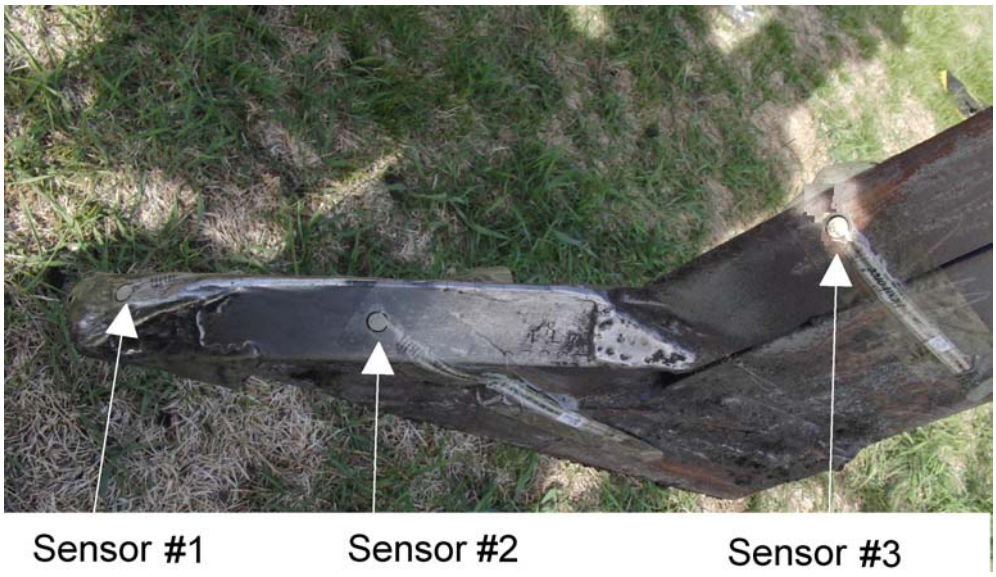

(b)

Fig. 5. Measurements of soil pressure; (a) Flexiforce film force sensor (after: www.tekscan.com); (b) locations of sensor installation on the ripper.

Soil loosening Soil loosening was defined as the change in soil porosity. The soil at the centre of a furrow has higher porosity than the soil in between two furrows where the soil may not be disturbed. Thus, measurements were performed at different lateral positions relative to the centre of furrow. Due to the difficulties in taking soil cores from disturbed soil (soil did not hold as cores), soil loosening was indirectly determined by measuring soil cone index (CI) using a cone penetrometer. The penetrometer (Model CP 20, Agridy Rimik pty. Ltd. Toowoomba, Australia) was comprised of an inbuilt data logger, an 800-mm long shift, a cone with a base area of 129 mm^2 and an apex angle of 30^o. The penetrometer was pushed into the soil by hands at a speed of approximately 30 mm s^{-1} according to ASABE (2006). CI was taken along a transect laid perpendicular to a furrow created by the ripper. The penetrometer was pushed into the soil at seven different lateral positions relative to the furrow, including at the centre of the furrow, 0.15,

0.30, and 0.45 m away from the furrow (Fig. 6). These measurements were performed to a depth of 0.4 m at 0.025 m depth intervals, at 10 random locations of the field.

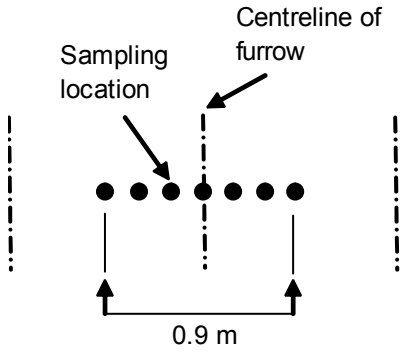

Fig. 6. Diagram showing sampling locations of soil cone index (CI); seven locations being equally distributed along a transect of 0.9 m.

To translate CI data into soil porosities, additional field measurements were performed to determine the relationship of CI and porosity. This was done by taking soil CI and soil cores at the same location for 20 locations in the field. Soil porosities determined by the soil cores were then correlated with soil cone indices.

Results of field measurements

Initial soil properties Average values of soil physical properties measured from the field test are listed in Table 2. The soil at the time of subsoiling had adequate moisture content (31.1% by mass) and bulk density (1330 kg/m^3). The average initial total porosity, 50% was derived from the initial bulk density and soil particle density (2560 kg/m^3). The gas filled porosity was determined by the total porosity and volumetric moisture content.

Table 2. Soil physical properties measured in the field.

Soil parameter	Gravimetric Moisture, %	Dry bulk density (kg/m^3)	Volumetric Moisture Content (m^3/m^3)	Total porosity (%)	Gas filled porosity (%)
Mean	31.1	1330	0.42	50	9
SD	3.1	121	0.07	5	1.1

Relationship between soil total porosity and cone index Values of the total soil porosity measured varied from 43 to 65%, which was within the range between 45 and 60% for clay reported by Koolen and Kuipers (1983). Data of soil total porosity and cone index were correlated (Fig. 7). There was a slightly decreasing trend of soil porosity with increasing cone index.

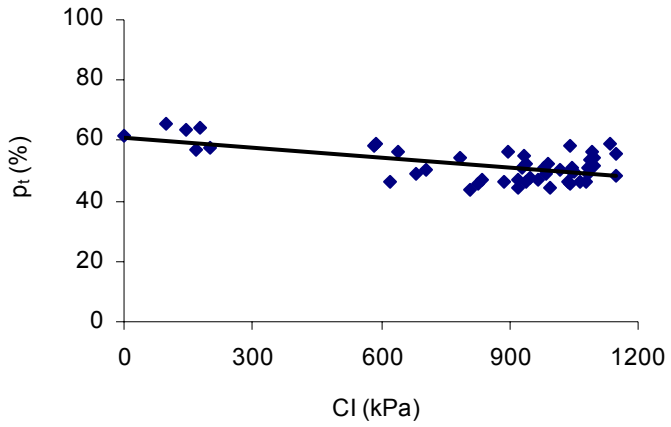

Fig. 7. Relationships between measured total soil porosity (p_t) and soil cone indices (CI).

A linear relationship between total soil porosity and cone index was generated from the data in Fig. 7 as

$$p_t = -0.011+61.17\ CI \tag{1}$$

where p_t is total soil porosity (%), CI is cone index (kPa). The low coefficient of determination (R^2=0.36) was expected due to the highly variable nature of soil.

With Eq (1) profile data of cone index taken at different depths and different lateral locations after subsoiling were converted to the corresponding profile data of total soil porosity which were used to determine the soil swell factor to assess the soil loosening of the ripper. Soil swell factor was defined as

$$SF = \frac{(p_t)_f - (p_t)_0}{(p_t)_0} \tag{2}$$

where SF is soil swell factor (%), $(p_t)_f$ is final (after subsoiling) total soil porosity (%), $(p_t)_0$ is initial (before subsoiling) total soil porosity (%). Fig. 8 shows the average values SF determined using Eq. (2) for 10 different locations of the field at different lateral positions crossing a furrow. These results will be used to validate the model results of soil loosening. This work will be presented in the future papers.

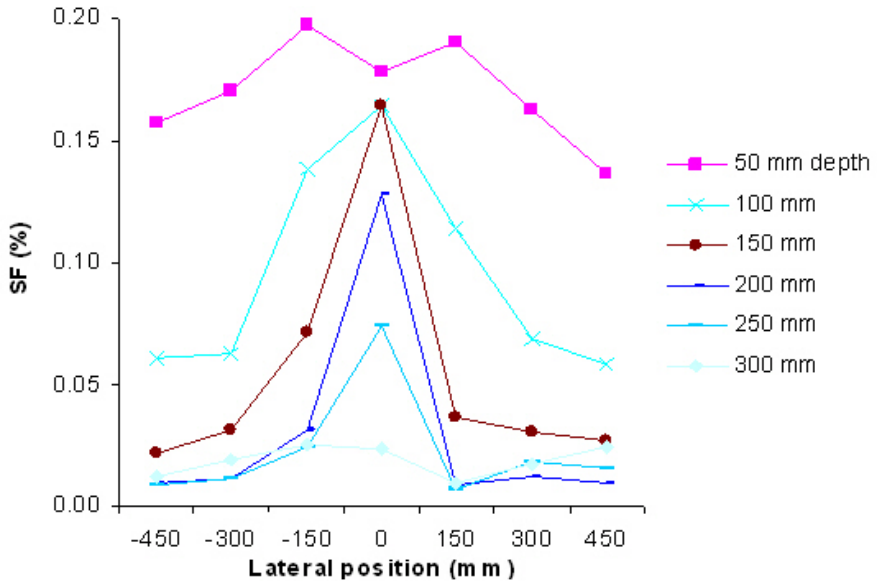

Fig. 8. Soil swelling factor (SF) estimated for different soil depths and different lateral positions relative to the centre of furrow.

Soil cutting pressure

The field result of sensor measurements was processed in order to use the data for calibrations in the PFC^{3D} model, in which the "wall sensors" detected only axial force resulted from wall-particles interactions. Therefore, after converting the force data recorded from each sensor to normal pressure format, the normal pressure was further projected to a plane to get the axial pressures (either XY plane, YZ plane, or XZ plane). It was assumed that the bottom of the ripper was perfectly parallel to the field ground surface and the shank was perpendicular to the ground surface. This would make the ripper shape being symmetrical along the travel direction. So that only one-time conversion was required for projecting the sensor pressure result to a two-dimension plane. The detailed conversion procedure and final average axial pressures on the projection planes are listed in Table 3.

Table 3. Data of field measurement with the sensors

Field measurement	Average normal pressure (Pa)	Projection plane	Pressure direction	Conversion coefficient	Average axial pressure (Pa)
Sensor #1	1.62E+06	XY plane	Z-Axis	cos(α)	8.91E+05
Sensor #2	1.07E+05	XZ plane	Y-Axis	cos(ρ)	9.54E+04
Sensor #3	3.35E+05	YZ plane	X-Axis	sin(β/2)	7.19E+04

PFC^{3D} SIMULATION

Particle generation and initial condition

A total of 160,434 particles were generated in the box (Fig. 9). Particles with radii in the range of 5 mm to 10 mm (representing the clay soil aggregate sizes) were uniformly distributed in the soil box (volume: 0.378 m^3) at the desired initial porosity, 25% (estimated soil macroporosity). The stress distribution within the box was isotropic due to the same properties definition of all the

particles within the box. The isotropic stress value under this model specific environment was 8.48×10^5 Pa. This value was determined by the input parameters, such as the Young's modulus of the particle and the walls, and the specified porosity, the latter of which affected the isotropic stress by scaling the particles sizes. Parallel bond were then installed to all the contacted particles with the appointed bond properties. The detailed procedure and principle of the particle generation used in the model are the same as those given by Potyondy and Cundall (2004).

Model computing

The model was run with the input parameters shown in Table 4. While model starts running, the tool moves in the soil box at a speed of 3 km/h and a tillage depth of 0.3 m. The overall runtimes of the model was about 60 hours. The model snapshot during running is shown in Fig. 9.

Table 4. Values and references of model parameters.

Parameter and symbol	Description and unit	Value	Source
Soil box			
W	width (m)	0.9	Equal to the tool spacing
H	Height (m)	0.6	Greater than the tillage depth
L	Length (m)	0.7	Travel distance
Soil particle			
R_1, R_2	Range of particle size (m)	0.010-0.015	Assumed
C	Soil cohesion (Pa)	10,000	ASAE (1994)
f_p / μ_p	Particle-particle friction angle (°)/coefficient	17.7/0.32	Koolen and Kuipers (1983)
E	Young's modulus (Pa)	6.8×10^7	Okunlola and Payne (1991)
$(K_n)_p$ and $(K_s)_p$	Normal and shear stiffness (N/m)	Calculated automatically	$(K_n)_p = 4RE$, R = particle radius
ρ_p	Bulk density (kg/m^3)	1330	Measured
Tool			
f_t / μ_t	Particle-tool friction angle (°)/coefficient	15.1/0.27	ASAE (1994)
$(K_n)_t$ and $(K_s)_t$	Tool stiffness (N/m)	1.0×10^9	Equal to steel stiffness
V	Tool ravel speed (km/h)	3	Same as the field test
D	Tillage depth (m)	0.3	Same as the field test
Parallel bond			
R_m	Radius multiplier	1.0	R_m = radius of smaller ball
τ_b	Bond shear strength (Pa)	10,000	Equal to cohesion, c
σ_b	Bond normal strength (Pa)	31,334	Equal to c×cot (Koolen and Kuipers, 1983)
E_b	Young's modulus (Pa)	10^4-10^9	Range used for calibration
$(K_n)_b$ and $(K_s)_b$	Normal and shear stiffness of bond (N/m)	Calculated automatically	$(K_n)_b = E_b/ (Ra + Rb)$

$(K_n)_b/(K_s)_b$	Bond stiffness ratio	2.5	Ra and Rb = particle radii PFC^{3D} default value

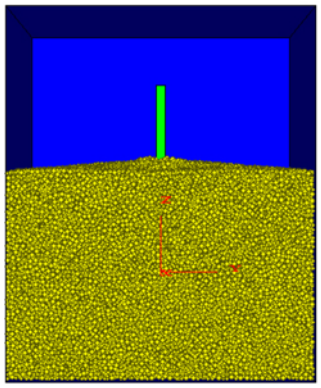

Fig. 9. Snapshot of the model during running (Back view of model)

Model calibrations

The model input parameter, Young's modulus of bond (E_b) is often difficult to measure, particularly at field scale, primarily due to the non-homogeneous nature of the soil. The inverse method was used to calibrate this parameter. Soil pressures were simulated using initial estimated parameter values and repeated simulation leading to the best match to the measured values. The virtual wall sensors were generated in the model with the similar locations as those in the real ripper (Fig. 10). The dimension and area of the three virtual sensors were listed in Table 5.

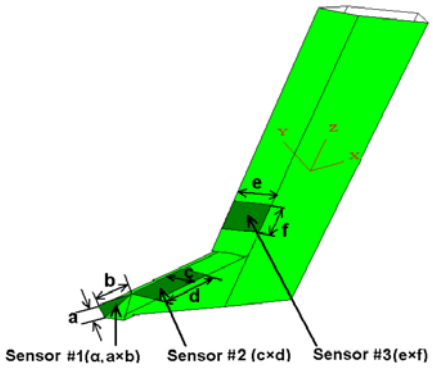

Fig. 10. Shape, location, and dimension symbols of the three "wall sensors" in the model.

Table 5. Shape, dimension and area of the virtual "wall sensors" in the model.

Wall sensors on the virtual ripper	Shape	Symbol and value (mm)	Area (mm^2)
Virtual wall sensor 1	Triangle	a = 30, b = 57	855
Virtual wall sensor 2	Parallelogram	c = 56, d = 81	2688
Virtual wall sensor 3	(Rectangular)	e = 70, f = 60	4200

Of all the results from the various model runs, the best matches between the measured soil pressures and the corresponding model outputs were shown in Fig. 11. The average value of the corresponding E_b should be between 10^5 Pa and 10^6 Pa, which will be taken as the bonding parameter for predictions of soil cutting forces and soil loosening in the future. The reason why there was a big difference on sensor 1 between field measurement and model output is not clear. Therefore, further researches on studying the effects of the Young's modulus of the parallel bond on the bond breakage and wall-particle interaction are required.

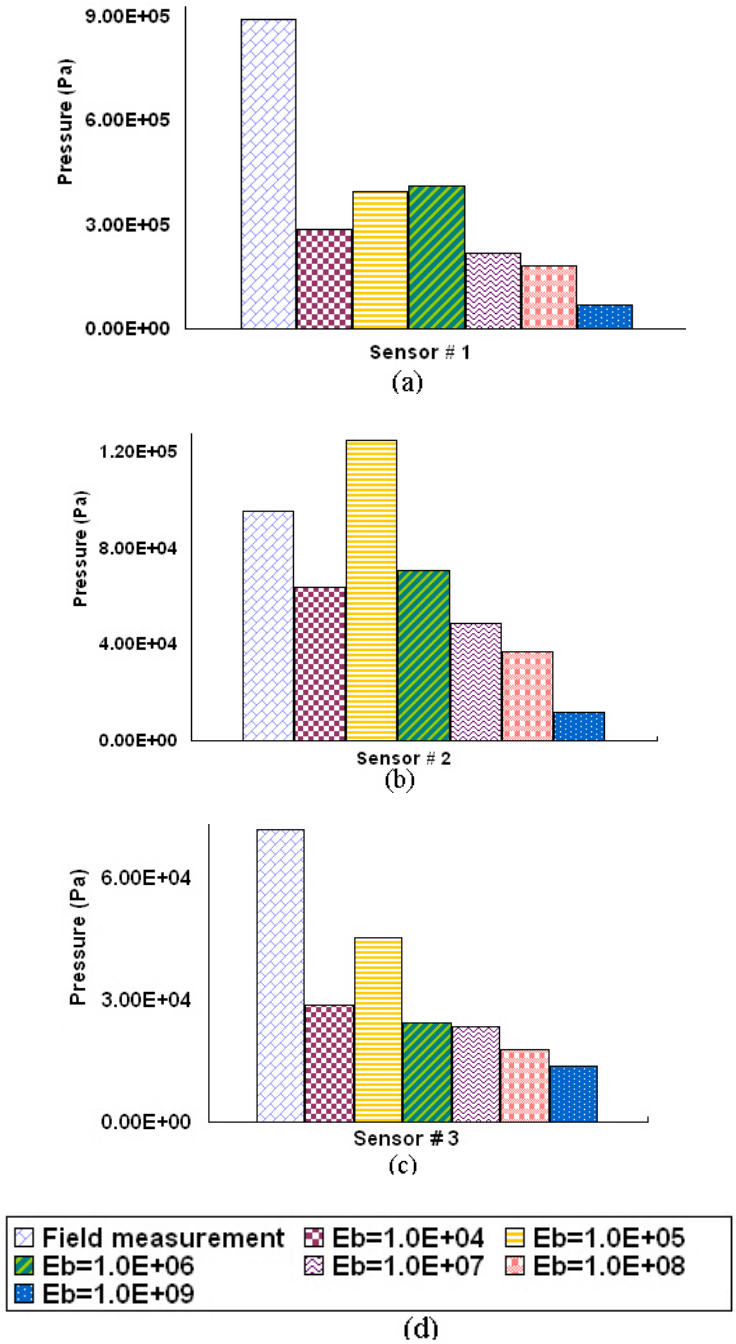

Fig. 11. Comparisons between field measurements and model outputs of (a) sensor # 1;(b) sensors # 2; (c) sensor # 3; (d) legend for the above three figures; Eb is Young's modulus of the parallel bond. Six model outputs are from the inputs of the six different Eb values.

CONCLUSION

PFC^{3D} was successfully used in the simulation of the soil cutting process of a ripper (subsoiling tool) working in a clay soil. The model allows the tool traveling at different speeds and working depths. This enhanced the understanding of the dynamic regime of the soil cutting process and the subsequent cutting forces and soil loosening.

A tillage tool, such as a ripper, could be constructed using the PFC^{3D} "wall" features. The parallel bonding model implemented in PFC^{3D} software seemed to be suitable to simulate the cohesive characteristics of a clay soil. When using this type of bonding, the PFC^{3D} fundamental particle shape, "balls" could be used to represent for soil particles. Soil aggregates, not individual soil particles, should be used as "particles" in PFC^{3D} when simulating agricultural clay soils. In this case, soil porosity in the PFC^{3D} model represents more for macroporosity than total porosity. The bond parameters between soil particles, which are not available, can be inversely calibrated with good matches between field measurements and the model outputs of soil cutting pressures on tool cutting surfaces. The model boundary and the ripper simulated had the field scale. Thus, the results can be directly applicable to field subsoiling.

Further work is to simulate soil cutting forces and soil loosening resulting from the ripper at different traveling speeds and tillage depths. The simulation results will be compared with results from analysis and measurements. Results describing the influence of the cutting depth and tool travel speed on the draft force will be very useful for choosing field operation parameters in order to minimize the energy requirement of subsoiling operations.

AKNOWLEGEMENT

The research was financially supported by Natural Sciences and Engineering Research Council of Canada (NSERC). Thanks are given to Jarrett Wylde for performing the field operation and to Carl Classen for providing the subsoiler. The help from Itasca (PFC^{3D} provider) technical staff Dr. David Potyondy is also highly appreciated.

REFERENCES

Anandarajah, A. 1994. Discrete-element method for simulating behaviour of cohesive soil. *Journal of Geotechnical Engineering*. 120(9): 1593-1613.

ASAE, 1994. *Advances in Soil Dynamics*. St. Joseph, MI: American Society of Agricultural Engineers.

ASABE Standards. 2006. ASAE Standard EP542. Procedures for using and reporting data obtained with the soil cone penetrometer. ASABE St. Joseph, MI 49805.

Botta, G.F., D. Jorajuria, R. Balbuena, M. Ressia, C. Ferrero, H. Rosatto and M. Tourn. 2006. Deep tillage and traffic effects on subsoil compaction and sunflower (*Helianthus annus L.*) yields. *Soil & Tillage Research* 91: 164-172.

Busscher, W.J., P.J. Bauer and C.R. Camp. 2006. Cotton management in a compacted subsurface mocroirrigated coastal plain soil of the southeastern US. *Soil & Tillage Research* 91: 157-163.

Chen, Y., C. Cavers, S. Tessier and D. Lobb. 2005. Short-term tillage effects on soil cone index and plant development in a poorly drained, heavy clay soil. *Soil & Tillage Research* 82(2): 161-171.

CSHM. 2008, Cornell Soil Health Manual. Department of Horticulture, College of Agriculture and Life Sciences, Cornell University, NY: Ithaca.

Chi, L. and R.L. Kushwaha. 1989. Finite element analysis of soil forces on different tillage tool shapes. ASAE/CSAE Paper No. 89-1103. St. Joseph, MI: ASAE.

Godwin, R.J. and G. Spoor. 1977. Soil failure with narrow tines. *Journal of Agricultural Engineering Research.* 22(4): 213-228.

Cundall, P.A. and O.D.L. Strack. 1979. A discrete numerical model for granular assemblies. *Geotechnique*. 29: 47-65.

Hettiaratchi, D.R.P. and A.R. Reece. 1967. Symmetrical three-dimensional soil failure. *Journal of Terramechanics*. 4(3): 45-67.

Itasca. 2005a. PFC^{3D} Particle Flow code in 3 Dimensions, Theory and Background. Itasca Consulting Group, Inc. Minneapolis, Minnesota, USA.

Itasca. 2005b. PFC^{3D} Particle Flow code in 3 Dimensions, User's Guide. Itasca Consulting Group, Inc. Minneapolis, Minnesota, USA.

Karlen, D.L., W.J. Bushcher, S.A. Hale, R.B. Dodd, E.E. Strickland and T.H. Garner. 1991. Drought condition energy requirement and subsoiling effectiveness for selected deep tillage implements. *Transaction of the ASAE.* 34: 1967-1972.

Koolen, A.J. and H. Kuipers. 1983. *Agricultural Soil Mechanics.* New York, NY: Springer-Verlag.

Landry, H., C. Laguë and M. Roberge. 2006. Discrete element modeling of machine–manure interactions. *Computers and Electronics in Agriculture*. 52: 90 – 106.

Liu, J., D. A. Lobb, Y. Chen, R. L. Kushwaha. 2008. Steady-State Models for the Movement of Soil and Straw during Tillage with a Single Sweep. *Transactions of the ASABE*. 51(3): 781-789.

Lu, Z., S.C. Negi and J.C. Jofriet. 1997. A numerical model for flow of granular materials in silos. Part 1: model development. *Journal of Agricultural Engineering Research.* 68: 223-229.

Mani, S., M. Roberge, L.G. Tabil and S. Sokhansanj. 2003. Modeling of densification of Biomass Grinds using discrete element method by PFC. CSBE Paper No. 03-207. Montreal, Quebec.

McDowell, G.R. and O. Harireche. 2002. Discrete element modelling of soil particle fracture. *Geotechnique.* 52 (2): 131-135.

McKyes, E. 1985. *Soil Cutting and Tillage*. Elsevier, New York.

McKyes, E. and O.S. Ali. 1977. The cutting of soil by narrow blade. Journal of Terramechanics 14(2): 43-58.

Okunlola, A. and D. Payne. 1991. Use of force-deformation curves to estimate Young's modulus and its applications to soil aggregate breakdown. *Journal of Soil Science*. 42(4): 543-549.

Perumpral, J.V., C.S. Grisso and C.S. Desai. 1983. A soil-tool model based on limit equilibrium analysis. *Transactions of ASAE.* 26(4): 991-995.

Potyondy, D. O. and P. A. Cundall. 2004. A Bonded-Particle Model for Rock. *International Journal of Rock Mechanics & Mining Sciences*. 41(8): 1329-1364.

Sakaguchi, F., M. Suzuki, J.F. Favier and S. Kawakami. 2001. Numerical simulation of the shaking separation of paddy and brown rice using the discrete element method. *Journal of Agricultural Engineering Research*. 79(3): 307-315.

Shen, J. and R.L. Kushwaha. 1998. *Soil-Machine Interactions*. New York, NY: Marcel Dekker Inc..

Shimizu, Y. and P.A. Cundall. 2001. Three-dimentioan DEM simulations of bulk handling by screw conveyors. *Journal of Engineering Mechanics*. 127(9): 864-872.

Tijskens, E., H. amon and J. De Baerdemaeker. 2003. Discrete element modeling for process simulation in agriculture. *Journal of Sound and Vibration*. 266(3): 493-514.

van der Linde, J. 2007. *Discrete Element Modeling of a Vibratory Subsoiler*. Matieland, South Acrica: Department of Mechanical and Mechatronic Engineering, University of Stellenbosch.